



Universiteit  
Leiden

The Netherlands

## Improving breast cancer outcome by preoperative systemic therapy and image-guided surgery

Mieog, J.S.D.

### Citation

Mieog, J. S. D. (2011, October 26). *Improving breast cancer outcome by preoperative systemic therapy and image-guided surgery*. Retrieved from <https://hdl.handle.net/1887/17983>

Version: Corrected Publisher's Version

License: [Licence agreement concerning inclusion of doctoral thesis in the Institutional Repository of the University of Leiden](#)

Downloaded from: <https://hdl.handle.net/1887/17983>

**Note:** To cite this publication please use the final published version (if applicable).

# Part II

---

## Image-guided surgery



# Part IIA

---

## Intraoperative tumor detection



# Chapter 8

---

## **Novel intraoperative near-infrared fluorescence camera system for optical image-guided cancer surgery**

Mieog JSD, Vahrmeijer AL, Hutteman M, van der Vorst JR, Drijfhout van Hooff M, Dijkstra J, Kuppen PJK, Keijzer R, Kaijzel EL, Que I, van de Velde CJH, Löwik CWGM

*Mol Imaging* 2010; 9:223-31

## ABSTRACT

### Introduction

Current methods of intraoperative tumor margin detection using palpation and visual inspection frequently result in incomplete resections, which is an important problem in surgical oncology. Therefore, real-time visualization of cancer cells is needed to increase the number of patients with a complete tumor resection. For this purpose, near-infrared (NIR) fluorescence imaging is a promising technique.

### Methods

Here, we describe a novel hand-held intraoperative NIR fluorescence camera system equipped with a 690 nm laser and validated its utility in detecting and guiding resection of cancer tissues in two syngeneic rat models. The camera system was calibrated using an activated cathepsin-sensing probe (ProSense).

### Results

Fluorescence intensity was strongly correlated with increased activated-probe concentration ( $R^2 = 0.997$ ). During the intraoperative experiments, a camera exposure time of 10 ms was used which provided the optimal tumor-to-background ratio. Primary mammary tumors ( $N = 20$  tumors) were successfully resected under direct fluorescent guidance. The tumor-to-background ratio was 2.34 using ProSense680 at 10 ms camera exposure time. The background fluorescence of abdominal organs in particular liver and kidney was high, thereby limiting the ability to detect peritoneal metastases with cathepsin-sensing probes in these regions.

### Conclusion

In conclusion, using this new camera system, we demonstrated its technical performance and intraoperative utility in guiding resection of tumors.

## INTRODUCTION

The main goal of surgical oncology is the complete and 'en-bloc' excision of tumors with adequate tumor-free margins whilst minimizing surgical morbidity. However, at present, intraoperative assessment of tumor margins is merely based on palpation and visual inspection, which frequently results in incomplete tumor resections (so-called R1 resections). For example, up to 40% of breast cancer patients treated with breast-conserving surgery needs to undergo secondary surgery due to involved tumor margins.<sup>1</sup> The local recurrence rate for primary or hepatic metastasis of colorectal carcinomas is 30-50% after curative intended surgery.<sup>2,3</sup> Breast and colorectal cancer are amongst the most commonly diagnosed types of cancer worldwide with each type responsible for more than a million new cases and half a million deaths annually.<sup>4</sup> For patients suffering from these cancers, surgery is the cornerstone of curative intended therapy. It is therefore clear that new visualization techniques are needed to facilitate intraoperative assessment of the extent of the cancer tissue and to guide the subsequent surgical removal of these tumors with adequate margins.

Optical imaging using near-infrared (NIR) fluorescence light has recently emerged as a promising technique to visualize cancer cells during surgery.<sup>5-9</sup> Advantages of NIR fluorescence light (700-900 nm) include: high tissue penetration up to several centimeters deep, low autofluorescence providing sufficient signal-to-noise ratio, the current availability of NIR fluorescence probes and labels for conjugation to target tumor-specific molecules, and the insensitivity of human eyes to NIR wavelengths providing no interference with the surgical field.<sup>6</sup> Nonetheless, only a small number of fixed-geometry or hand-held fluorescence imaging systems have been developed with surgical oncology in mind.<sup>10-15</sup> These systems employ either a laser light source<sup>10,13</sup> or light emitting diodes (LED)<sup>11,12</sup> for NIR fluorescence excitation. Gutowski *et al.*<sup>10</sup> assessed the technique of intraoperative immunophotodetection using a prototype device (BFP Electronique, France). In this device, a cooled laser diode emitted light at 649 nm through a fiber-optic output. Ke *et al.*<sup>13</sup> used a custom built imaging system for intraoperative tumor detection, which employed two laser diodes at 660 nm (0.7mW/cm<sup>2</sup>) and 785 nm (1.6mW/cm<sup>2</sup>). Images were enhanced using an image intensifier tube. Kirsch *et al.*<sup>14</sup> described the use of a handheld device (Siemens Medical Solutions, USA), for which they described the molar detection limit. The Photodynamic Eye (PDE, Hamamatsu Photonics, Japan) uses LEDs and is designed for the detection of the clinically available probe indocyanine green and has been used in several clinical studies on lymph node mapping<sup>12,16,17</sup> and tumor imaging.<sup>9</sup> The system provides 1 mW/cm<sup>2</sup> of 760 nm excitation light. The FLARE™ imaging system has been used in preclinical<sup>18-20</sup> and clinical studies.<sup>15</sup> This system employs high power, cooled LEDs at 670 nm (4 mW/cm<sup>2</sup>) and 760 nm (14 mW/cm<sup>2</sup>) and also uses spectrally separate white light LEDs to illuminate the surgical field. This three-channel approach has the great advantage of displaying the NIR fluorescence signal in direct relation to the anatomical

landmarks by superimposing the NIR fluorescence image on the visible light image. However, the FLARE™ is significantly larger than other, hand-held systems.

All systems use charge-coupled devices (CCD) for signal registration. As the quantum efficiency of CCDs tends to diminish significantly in the NIR spectrum, the choice for a specific CCD is, besides excitation light and quality of optics, of importance for the detection limits of an imaging system. However, technical details such as illuminating power, detection capabilities of the camera, and resolving power are not clearly described for all of the above described camera systems. In order to determine an imaging system's contribution to the field of NIR fluorescence image-guided surgery, a system needs to be analyzed in a well-structured way for its technical capabilities (i.e. NIR excitation light production, detection limits) and its practical use (i.e. ergonomics, sterility).

Here, we describe the Fluobeam®, a novel, hand-held, intraoperative fluorescence camera system. The minimal detection limits, resolving power and intraoperative utility are addressed in primary breast cancer and metastatic colorectal cancer in two syngeneic rat models.

## MATERIAL AND METHODS

### Near-infrared fluorescence camera system

The Fluobeam® system (Fluoptics, Grenoble, France) is composed of a class 3B continuous wave laser (100 mW) emitting at 690 nm (Power Technology, USA) and supplied by a mains supply box (Mascot, Norway) continuously delivering 9V output current with a maximum of 4.5 A. The light from the excitation source is scattered using a diffuser in order to produce a homogeneous lightened field (6-8 cm diameter, field homogeneity > 30%) with an illumination power of 2.6 mW/cm<sup>2</sup>. The animal is placed under the laser and illuminated by white light (Photonic Optics, China) filtered with a band-pass filter (350-650 nm) providing an irradiance of  $7 \times 10^3$  lx at the animal level. The fluorescence signal is collected through a long pass filter (> 700 nm, OD-value at 690 nm is 3.5) by a digital 12-bit CCD camera (PCO Imaging, Germany) using a fixed-focus objective (Schneider Optische Werke GmbH, Germany). Camera exposure times are adjustable between 1 to 1000 ms. Camera exposure times of 10 ms and 20 ms provided the best contrast between tumor and background during surgical exploration for ProSense680 and ProSense750, respectively, and were used during both the *in vitro* and the *in vivo* part of this study. The spatial resolution of the Fluobeam is 0.17 mm/pixel at focus point. The resolving power of the system is 2.52 line pairs per mm, as determined using the USAF 1951 Target. The laser, the filtered white light illumination and the camera are suspended on a multi-angle adjustable arm which is positioned 20 cm above the point of focus allowing sufficient space for

surgical maneuvers (Figure 1). The system is operated by a desktop computer and the fluorescence signal is displayed in real-time on the computer screen.

### NIR fluorescence probe

The NIR fluorescence probes ProSense680 and ProSense750 (VisEn Medical, Woburn, USA) with peak absorbance of 680 and 750 nm, respectively, were used for fluorescent imaging. ProSense is an autoquenched fluorescent probe that converts from a non-fluorescent to a fluorescent state by proteolytic activation of lysosomal cysteine or serine proteases like cathepsin-B.<sup>21</sup>

### Calibration of camera system

For calibration of the Fluobeam camera system, 2 nmol Prosense (150  $\mu$ l) was activated with 100  $\mu$ l 0.25% trypsin-EDTA at 37 °C for 1 h.<sup>14</sup> The cleaved probe was diluted to a concentration of 128 nM and diluted 10 times on the ratio 1:2 in phosphate buffered saline and aliquoted into a 96 wells plate (Greiner Bio-one, #655090, suitable for fluorescent measurements). Subsequently, the samples were imaged with the Fluobeam at various camera exposure times. The experiment was performed for both ProSense680 and ProSense750. Phosphate buffered saline was used as negative control. In order to confirm the accuracy of dilution, the same samples were measured using the Odyssey NIR fluorescence scanning device (LI-COR Biosciences, USA).

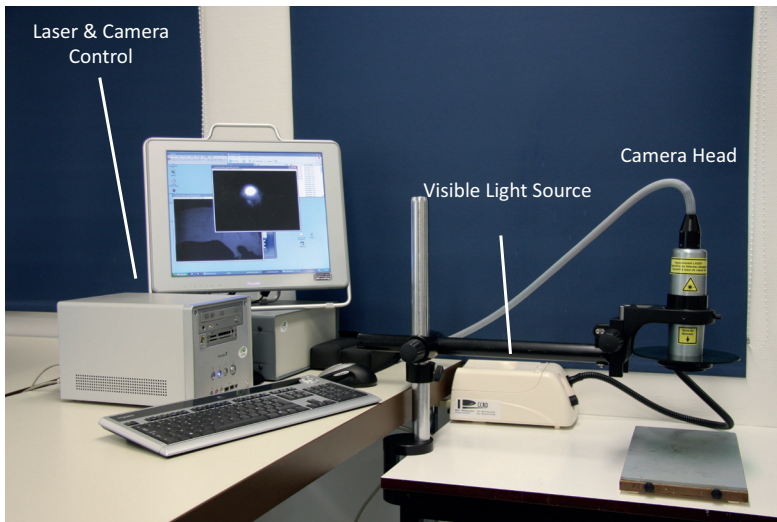


Figure 1. The Fluobeam® intraoperative near-infrared camera system

## Cell line experiments

The syngeneic MCR86 breast cancer rat cell line and the syngeneic CC531 colorectal cancer cell line were used for cell line experiments.<sup>22, 23</sup> Tumor cells were cultured in RPMI 1640 supplemented with 2 mM L-glutamine (Gibco, USA), 10% heat-inactivated fetal calf serum, 100 U/ml penicillin and 0.1 mg/ml streptomycin sulphate. Cells were harvested with a solution of 0.25% (w/v) EDTA and 0.25% (w/v) trypsin in HBSS (Sigma, St. Louis, MO, USA).

In order to determine the minimal number of tumor cells that could be detected, MCR86 and CC531 tumor cells were cultured in T75 culture flasks up to  $\frac{3}{4}$  confluence and incubated in 20 ml medium with 10 nM ProSense680. After 24 h incubation with ProSense680, cells were washed, harvested as described above, washed in medium and adjusted to a suspension containing  $1 \times 10^6$  tumor cells per ml. This suspension was diluted 7 times on the ratio 1:2 in medium and aliquoted in 1.5 ml tubes. Tubes were centrifuged at 13,000 rpm for 5 minutes to generate cell pellets. Subsequently, the cell pellets were imaged with the Fluobeam at 10 ms camera exposure time. Tumor cells incubated with medium only served as negative control. This experiment was repeated three times for both the MCR86 and CC531 cell lines.

## Animal models

### *EMR86 breast cancer rat model*

The syngeneic transplantable EMR86 breast cancer model originated in a female WAG/Rij rat bearing a subcutaneously implanted estrogen pellet and is related to the MCR86 cell line. This model is developed by our research group.<sup>24</sup> Tumors are only induced and maintained in rats carrying estrogen pellets, whereas tumors transplanted into non-estrogenized animals never grow out. Fresh EMR86 tumor fragments of  $1 \text{ mm}^3$  were subcutaneously implanted into the mammary fat pads at four sites in 4-6 months old female WAG/Rij rats (Charles River, the Netherlands). Simultaneously, an estrogen pellet was implanted subcutaneously in the intrascapular region of the neck. The in-house generated pellets consist of 2 by 3 mm silicone tubes containing 1.5 mg 17 beta-estradiol on a 1:3 cholesterol/ paraffin basis. Tumor volumes were estimated using digital calipers by measuring three orthogonal diameters of the tumor and multiplying this product by  $\pi/6$ . After four weeks, tumors had reached of volume of approximately  $1 \text{ cm}^3$ .

### *CC531 colorectal cancer rat model*

In order to induce CC531 peritoneal metastases, CC531 cells were harvested as described above, washed three times in phosphate buffered saline and adjusted to a

suspension containing  $2 \times 10^6$  viable (trypan blue exclusion test) tumor cells per ml. The peritoneal cavity was inoculated with  $2 \times 10^6$  cells in 6-months old male WAG/Rij rats (Charles River, the Netherlands).<sup>25</sup> Two weeks after inoculation, small metastases of approximately 2 mm in diameter have originated in the abdominal cavity.

### Animal experiments

All animals were housed in the animal facility of the Leiden University Medical Center. Pellet food and fresh tap water were provided *ad libitum*. The weight of the animals was followed throughout the experiment to monitor their general health state. Throughout imaging and surgical procedures, the animals were anesthetized with 5% isoflurane for induction and 2% isoflurane for maintenance in oxygen with a flow of 0.8 L/min and placed on animal bed with integrated nose mask. The Animal Welfare Committee of the Leiden University Medical Center approved these studies.

Rats were injected with ProSense (i.v., 10 nmol per animal) 24 hours before imaging. Before injection, autofluorescence of tumors, surrounding tissue and abdominal organs was determined. Rats were shaved to reduce absorption of the optical signal by fur. Animals were anesthetized with isoflurane as described above. Ethanol 70% was used as a disinfectant. EMR86 mammary tumors were removed by making an incision ventrally of the tumor and carefully dissecting the tumor with direct guidance of the real-time fluorescent signal. For the detection of CC531 intra-peritoneal metastases, a median laparotomy was performed followed by a systematic exploration of the small and large bowel along with the mesentery and peritoneal cavity. Metastases identified clinically or by fluorescence were carefully excised. Fluorescent intensity of tumors and abdominal organs was determined *in vivo* and *ex vivo* using the Fluobeam. Excised tumors were snap frozen in isopentane and stored at  $-80^\circ\text{C}$  or fixed in formaline and embedded in paraffin (FFPE) blocks. Frozen tissue sections of 20  $\mu\text{m}$  or FFPE tumor sections of 4  $\mu\text{m}$  were air-dried and stained with hematoxylin and eosin.

### Statistical analysis

Fluobeam derived NIR fluorescence data were analyzed using the open-source software ImageJ by drawing regions of interest and measuring the fluorescent intensity of the 12-bit images.<sup>26</sup> For determination of detection limits, the fluorescent intensity of test samples was divided by the fluorescent intensity of the negative control. A ratio higher than 2 was considered as discriminative. For the animal experiments, regions of interest were drawn at the tumor and at the surrounding tissue within a range of 2 mm of the demarcation line of the tumor and the surrounding tissue. Statistical analysis and generation of graphs was performed using GraphPad Prism software (version 5.01, California, USA). Unless otherwise stated, mean fluorescent intensity

and associated standard deviations were reported. Pearson's correlation coefficients  $R^2$  were used for the *in vitro* experiments. Unpaired and paired *t*-tests were used for testing differences of continuous variables between groups. Statistical tests were two-tailed and  $P < .05$  was considered significant.

## RESULTS

### Calibration of camera system

Trypsin-activated ProSense680 and ProSense750 were used to calibrate the Fluobeam camera system (Figure 2A). Fluorescent intensity was linearly correlated with the concentration of activated ProSense680 and ProSense750 (correlation coefficient  $R^2 = 0.997$  and  $0.997$ , respectively). The dilution accuracy was confirmed using the Odyssey NIR fluorescence scanning device for both ProSense680 ( $R^2 = 0.995$ ) and ProSense750 ( $R^2 = 0.995$ ). At similar Fluobeam camera exposure times, fluorescent intensity of ProSense680 was on average 2.6 times higher than the fluorescent intensity of ProSense750. This reflects the better matching of the absorbance peak of ProSense680 with the 690 nm emitted by the laser of the Fluobeam. Therefore, ProSense680 was used in subsequent *in vitro* experiments. Camera exposure time was linearly correlated with fluorescent intensity ( $R^2$  ranged between 0.997 and 1 for the different concentrations), indicating linearity of the camera system. During the *in vivo* experiments, the optimal fluorescent signal for tumor identification without saturated pixels was obtained at 10 ms camera exposure time. Therefore, a 10 ms camera exposure time was used during subsequent *in vitro* experiments using ProSense680. In order to quantify the sensitivity of the camera system, the minimal detectable concentration of

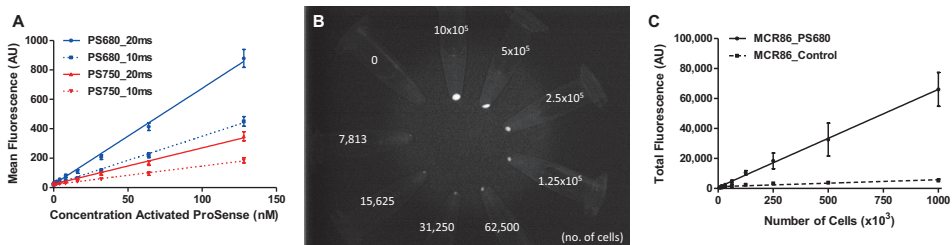


**Figure 2. Calibration of the Fluobeam® camera system.** A. The concentration of trypsin-activated ProSense680 and ProSense750 is plotted against the mean fluorescent intensity at 10 and 20 ms camera exposure times. B. NIR fluorescence Fluobeam image showing 1.5 ml tubes containing cell pellets of various amounts of cells of the MCR86 breast cancer cell line after 24 h incubation with 10 nM ProSense680. Camera exposure time was 10 ms. C. The number of MCR86 cells incubated with 10 nM ProSense680 is plotted against the total fluorescent intensity at 10 ms camera exposure time.

ProSense680 was determined at 10 ms camera exposure time, mimicking the *in vivo* situation. A signal-to-background ratio was calculated with phosphate buffered saline as background. A ratio of 2 was used as the cut-off. At these settings, the minimal detectable concentration of trypsin-activated ProSense680 was  $9.3 \pm 0.1$  nM (Figure 2A). Therefore, a concentration of 10 nM was used in subsequent cell line experiments.

### Cell line experiments

In order to determine the minimal number of tumor cells that could be detected with the Fluobeam and ProSense680, cultured MCR86 and CC531 tumor cells were incubated in medium with 10 nM ProSense680. After 24 hours incubation, cells were aliquoted in 1.5 ml tubes at various cell concentrations, spun down and imaged with the Fluobeam (Figure 2B). The total fluorescence of the cell pellets was linearly correlated with the number of cells at 10 ms camera exposure time for both MCR86 ( $R^2 = 0.952$ ; Figure 2C) and CC531 ( $R^2 = 0.989$ ; data not shown). To determine the minimal detection limit, a signal-to-background ratio was calculated with medium only as background. A ratio of 2 was used as the cut-off. At 10 ms camera exposure time, the minimal detection limit of the Fluobeam was  $20,400 \pm 9,200$  MCR86 cells and  $12,800 \pm 2,700$  CC531 cells (data not shown). Cell pellets containing 20,000 cells are approximately  $0.2 \text{ mm}^3$ , reflecting sub-mm metastases.

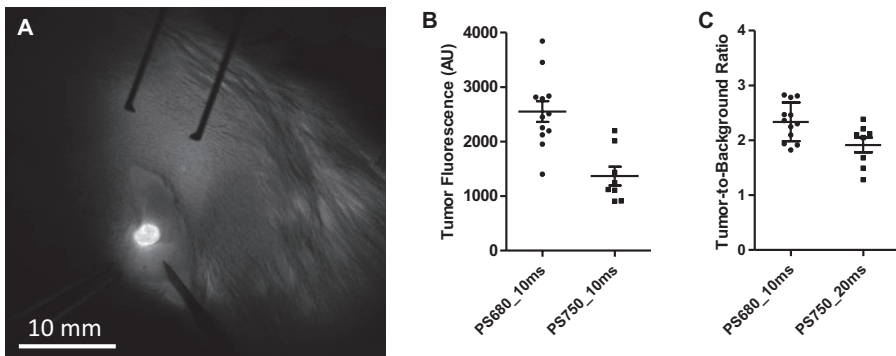


**Figure 3. Intraoperative NIR fluorescence guided resection of primary breast cancer using the Fluobeam® camera system.** A. NIR fluorescence image showing the intraoperative view of a 3.5-mm EMR86 breast tumor in a female rat 24 h after administration of 10 nmol ProSense680. Camera exposure time was 10 ms. B. The mean fluorescent intensity of breast tumors is plotted for ProSense680 (N = 12 tumors, 3 rats) and ProSense750 (N = 8 tumors, 3 rats). Camera exposure time was 10 ms. Horizontal lines represent mean  $\pm$  SD. Fluorescent signal of the tumors was higher with ProSense680 than with ProSense750 ( $t = 4.33$ ,  $P = .0004$ ). C. The tumor-to-background ratio is plotted for both ProSense680 (N = 12 tumors, 3 rats) and ProSense750 (N = 8 tumors, 3 rats) for the camera exposure times that provided the optimal tumor-to-background ratio during surgery: 10 ms for ProSense680 and 20 ms for ProSense750. Horizontal lines represent mean  $\pm$  SD. Tumor-to-background ratio was significantly higher for ProSense680 when compared to ProSense750 ( $t = 2.53$ ,  $P = .021$ ).

## Intraoperative imaging

### Primary breast cancer

The syngeneic EMR86 breast cancer rat model was used to test the intraoperative application of the Fluobeam camera system. Primary breast tumors were induced in six female rats in the mammary fat pad. Twenty tumors were induced varying in size from 0.08 to 4.19 cm<sup>3</sup> (mean = 0.77 cm<sup>3</sup> ± 1.4). All tumors were successfully detected and resected under direct fluorescence guidance 24 hours after injection with ProSense680 (N = 12 tumors) or ProSense750 (N = 8 tumors, Figure 3). In concordance with the *in vitro* data, the fluorescent signal of the tumors was higher with ProSense680 (mean = 2552 ± 659.4) than with ProSense750 (mean = 1367 ± 489.9;  $t = 4.33$ ,  $P = .0004$ ; Figure 3B) at a 10 ms camera exposure time. During surgery, an optimal fluorescent contrast between tumor (unsaturated signal) and surrounding mammary fat pad was obtained using a 10 ms camera exposure time for ProSense680 and 20 ms for ProSense750. The signal of ProSense680 was stronger due to better matching with the 690 nm laser, as

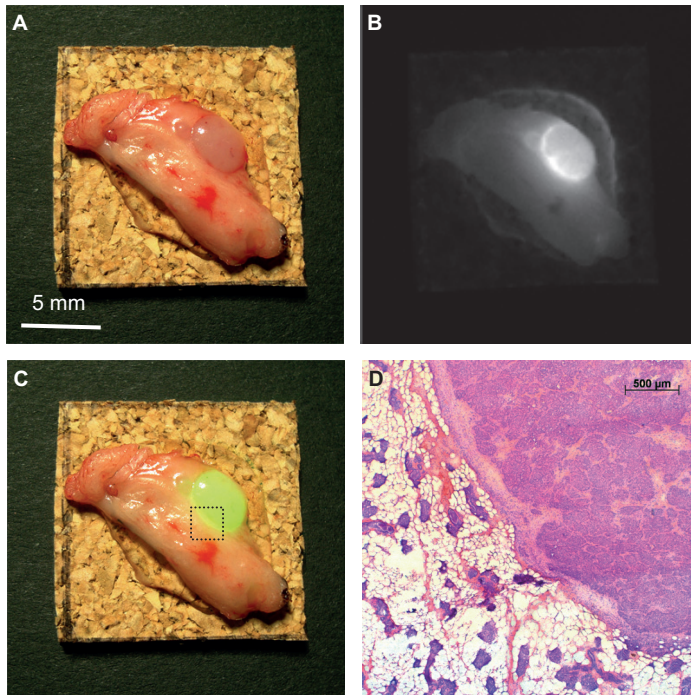


**Figure 4.** NIR fluorescence imaging of excised primary breast cancer using the Fluobeam® camera system. Shown are a color image (A), a NIR fluorescence image (B), and a pseudocolored green merge of the two images (C) of a sectioned 4-mm EMR86 breast tumor with surrounding mammary fat pad. The tumor was excised from a rat, which was injected with 10 nmol ProSense680 24 h prior to imaging. Camera exposure time was 10 ms. D. H&E histological staining of a 20 µm frozen tissue section of the specimen from Figure 4C. Shown is the region indicated by the dashed square (25x magnification).

discussed above. Although the fluorescent intensity of tumor tissue was significantly higher than the surrounding mammary fat pad with both ProSense680 (paired  $t = 12.52$ ,  $P < .0001$ ,  $N = 12$  tumors) and ProSense750 (paired  $t = 6.29$ ,  $P = .0004$ ,  $N = 8$  tumors) using these camera exposure times, the tumor-to-background ratio was significantly higher for ProSense680 ( $2.34 \pm 0.35$ ) when compared to ProSense750 ( $1.91 \pm 0.38$ ;  $t = 2.53$ ,  $P = .021$ ; Figure 3C).

### *Breast tumor margins*

In order to visualize the fluorescence of tumor margins, excised breast tumors were sectioned, imaged with the Fluobeam and processed for histopathology. In Figure 4, a typical example of a 4 mm large excised breast tumor is presented. A distinctive difference in fluorescence of the tumor tissue and surrounding mammary fat pad is shown which is confirmed in a fresh frozen tissue section after hematoxylin and eosin staining.

### *Metastatic abdominal cancer*

To assess if the use of a protease-activatable probe could be used in tumor types located in the abdominal cavity, the fluorescence intensity of abdominal organs relevant in cancer surgery was measured with the Fluobeam in three rats before and after injection with ProSense680. Figure 5 demonstrates that liver, kidney, spleen, small bowel and

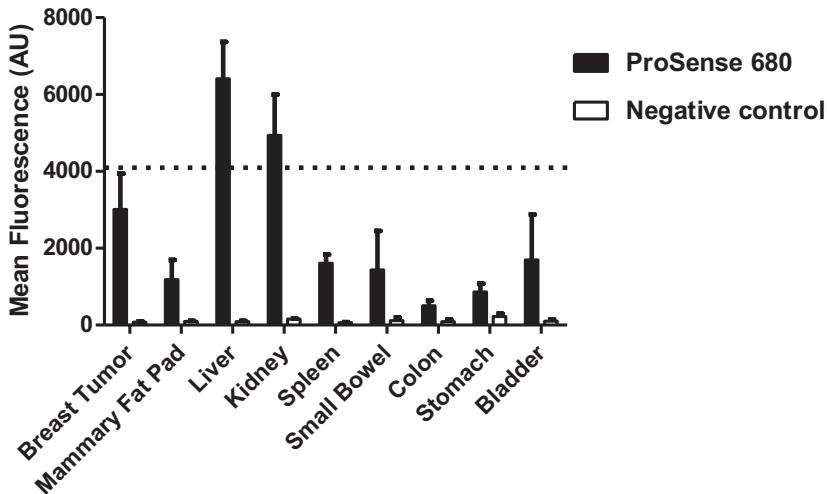


**Figure 5.** *In vivo* fluorescence intensity of EMR86 breast tumors and abdominal organs. Fluorescent intensity was measured using the Fluobeam® camera system in three rats bearing EMR86 breast tumors before and 24 h after administration of 10 nmol ProSense680. Camera exposure time was 10 ms. Bars represent mean  $\pm$  SD. The signal for liver and kidney was saturated at 10 ms camera exposure times (dashed line). The plotted values are extrapolated from the non-saturated measurements at 5 ms camera exposure time.

bladder provide very high background fluorescence after injection of ProSense680. The fluorescent intensity of liver tissue was 69 times higher than in control rats ( $t = 8.85$ ,  $P = .003$ ) reflecting the high intrinsic cathepsin B activity of hepatocytes.<sup>27</sup> Also, the signal in the kidney was 32 times higher in the ProSense680 rats, particularly in the renal cortex, due to the intrinsic cathepsin B activity and the renal clearance of the probe ( $t = 6.06$ ,  $P = .009$ ).<sup>28</sup> Similar results were obtained with ProSense750.

These results suggest that protease-activatable probes are less useful for image-guided surgery of abdominally located tumors or metastases regardless of the protease activity and associated fluorescent intensity of those tumors.

To test the assumption that the use of ProSense in detecting abdominal tumors is limited, the syngeneic CC531 colorectal cancer rat model was used to induce intra-peritoneal tumors. Figure 6 shows a typical example of a rat bearing intra-peritoneal CC531 metastases imaged with the Fluobeam after injection with ProSense750. Although small peritoneal metastases could be detected on the mesentery of the small bowel (Figure 6A-B), one can not be sure to detect metastases in all parts of the bowel and in particular at the liver and kidney due to the high background fluorescence, as illustrated in Figure 6C.

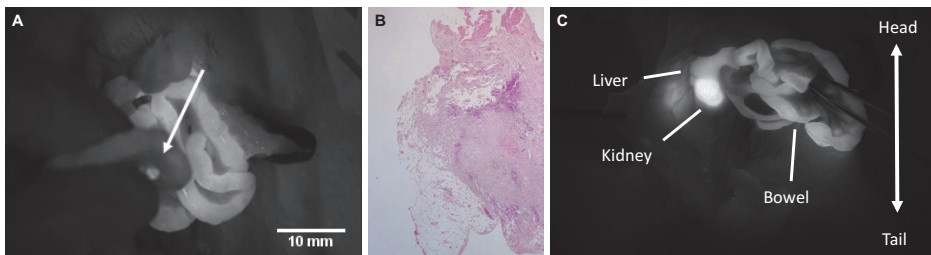


**Figure 6.** Intraoperative NIR fluorescence imaging of colorectal CC531 peritoneal metastases using ProSense and the Fluobeam® camera system. **A.** NIR fluorescence image showing a 3-mm fluorescent hotspot (arrow) located on the mesentery of the small bowel in a male rat injected with 10 nmol ProSense750. Camera exposure time was 20 ms. **B.** Corresponding H&E-stained formaline-fixed paraffine-embedded 4  $\mu$ m tissue section confirms the presence of CC531 tumor cells (original magnification 25x). **C.** Intraoperative NIR fluorescence image showing the background fluorescence of the liver, kidney and small bowel in the same animal. Camera exposure time was 20 ms.

## DISCUSSION

A highly promising new development in surgical oncology is image-guided tumor resection using NIR fluorescence imaging. The extent of the primary tumor as well as sites of regional disseminated disease can be detected in real-time. Using this new information, the surgical procedure can directly be adapted. Moreover, this technique provides a direct assessment of the resection plane after tumor removal to detect any residual cancer tissue, thereby reducing the number of patients with incomplete tumor resections. However, NIR fluorescence imaging with tumor-specific probes has not

been evaluated in humans. The main target of ProSense, the cysteine protease family (in particular cathepsin B) is upregulated in various human cancers including breast and colorectal cancer.<sup>29-32</sup> In the current pre-clinical study, we described the performance of a novel hand-held, intraoperative NIR fluorescence camera system based on a 690 nm laser and demonstrated its utility in detecting and guiding resection of primary and metastatic rat tumors using the cathepsin-activatable probe ProSense. Because the family of proteases is strongly conserved amongst mammals, it is expected that ProSense will be applicable for cancer patients.<sup>29</sup>

The efficacy of NIR fluorescence camera systems is determined by the interplay between the type of probe used, the probe concentration, tumor size and the camera exposure time. In this study, the cathepsin-activatable probe ProSense680 and ProSense750 were used to test the 690 nm laser-based Fluobeam camera system. Because of the better matching of ProSense680 with the 690 nm laser, the fluorescent signal was significantly higher using ProSense680 (Figure 2A). During the intraoperative experiments, 10 ms camera exposure time was found to be optimal in terms of tumor-to-background ratio for ProSense680. When assessed *in vitro*, the minimal detectable ProSense680 concentration at 10 ms camera exposure time was approximately 10 nM (Figure 2A). The minimal detectable number of tumor cells with 10 nM ProSense680 at 10 ms camera exposure time was approximately 20,000 for a breast cancer cell line and 13,000 for a colorectal cancer cell line. These cell numbers reflect sub-mm tumor depositions. When these settings were applied in the *in vivo* experiments, mammary tumors varying in size from 0.08 to 4.19 cm<sup>3</sup> could be detected and subsequently resected under direct fluorescent guidance after administration of 10 nmol ProSense680 with a clear demarcation of tumor margins (Figure 4). Fluorescence reflectance imaging is not inherently quantitative and quantification should always be performed relative to control tissue.<sup>5</sup> In this study, a tumor-to-background ratio of 2.34 was found for ProSense680. Tumor tissue was discriminated from the surrounding tissue by optimal thresholding without any further signal improvement techniques.<sup>33</sup>

In general, the ratio of the fluorescent intensity between tumor and surrounding tissue determines the applicability of protease-activatable probes in NIR fluorescence image-guided cancer surgery. In order to assess the applicability of the cathepsin-sensing probe in intraperitoneal metastases, the fluorescent intensity of abdominal organs were measured after the administration of ProSense680. In several abdominal organs the fluorescent intensity was markedly increased after injection of ProSense (Figure 5). For example, liver, kidney and intestine cells exploit an extensive cathepsin B activity and were highly fluorescent.<sup>27</sup> Therefore, cathepsin-activatable probes seem less useful for image-guided surgery of abdominally located tumors, even if tumors express high levels of cathepsin-B (Figure 6).

The currently available NIR fluorescence camera systems use either a laser<sup>13,14</sup> or light emitting diode (LED)<sup>11,12,19</sup> illumination as a photon source for probe excitation.

The Fluobeam camera system is laser-based, which might possess logistic hurdles in terms of operator safety, although a distance of 18 cm away from the camera head is considered safe. However, LED illumination requires direct cooling at the camera head causing camera heads to be larger. Conversely, a fiber-guided laser source can be cooled outside the camera head, therefore the camera head can be smaller and a true hand-held system can be created. Direct comparison of various camera systems is necessary to test accuracy and efficacy parameters such as minimal detection limit, excitation power and signal-to-noise ratio in a standardized way, as presented here. Advantages of the Fluobeam system include its compact size, high resolving power and spatial resolution, user friendly and surgeon-oriented mode of operation, and the fact that the Fluobeam is commercially available. Moreover, the software incorporates the use of a dynamic threshold function, which could enhance the discrimination of tumor and normal tissue. Improvements of the Fluobeam could include the addition of a color video camera for visible light registration, as is already implemented in the LED-based FLARE™ system.<sup>15</sup>

Several new developments in optical imaging, such as fluorescence lifetime imaging,<sup>34</sup> frequency domain imaging and spatially modulated structured light<sup>35</sup> have the potential to increase tissue penetration and discriminatory power between fluorophores. These techniques are able to improve localization of an NIR fluorescence signal source and improve quantification of the fluorescence signal. These developments are expected to be integrated in intraoperative NIR fluorescence imaging devices within the next few years.

In conclusion, the ultimate goal of NIR fluorescence imaging is to provide surgical oncologists with a real-time tumor imaging technique to guide surgery for the complete and safe resection of cancer tissue. In this study, we described the technical details and performance of the Fluobeam intraoperative NIR fluorescence camera system. By using the Fluobeam and the activatable probe ProSense, we demonstrated that it is possible to resect tumors under fluorescence guidance. If these techniques will become available for clinical cancer treatment, surgical oncology will make a major step forward.

## ACKNOWLEDGEMENT

We want to thank Fluoptics (Grenoble, France) for providing us with the Fluobeam® system to perform the above described experiments and Gabi van Pelt for technical assistance. This study was performed within the framework of CTMM, the Center for Translational Molecular Medicine. DeCoDe project (grant 03O-101). This study was supported by the Sacha Swarttouw-Hijmans Foundation. J.S.D. Mieog is a MD-medical research trainee funded by the The Netherlands Organisation for Health Research and Development (grant nr. 92003526).

## REFERENCES

1. Verkooijen HM, Borel RI, Peeters PH, et al. Impact of stereotactic large-core needle biopsy on diagnosis and surgical treatment of nonpalpable breast cancer. *Eur J Surg Oncol* 2001; 27:244-9.
2. Nagtegaal ID, van de Velde CJ, Marijnen CA, et al. Low rectal cancer: a call for a change of approach in abdominoperineal resection. *J Clin Oncol* 2005; 23:9257-64.
3. Finch RJ, Malik HZ, Hamady ZZ, et al. Effect of type of resection on outcome of hepatic resection for colorectal metastases. *Br J Surg* 2007; 94:1242-8.
4. Ferlay J, Bray F, Pisani P, Parkin D. *GLOBOCAN: Cancer Incidence, Mortality and Prevalence Worldwide*. 1st edn. Lyon: IARCPress; 2001.
5. Weissleder R, Pittet MJ. Imaging in the era of molecular oncology. *Nature* 2008; 452:580-9.
6. Frangioni JV. New technologies for human cancer imaging. *J Clin Oncol* 2008; 26:4012-21.
7. Kaijzel EL, van der Pluijm G, Lowik CW. Whole-body optical imaging in animal models to assess cancer development and progression. *Clin Cancer Res* 2007; 13:3490-7.
8. Stepp H, Beck T, Pongratz T, et al. ALA and malignant glioma: fluorescence-guided resection and photodynamic treatment. *J Environ Pathol Toxicol Oncol* 2007; 26:157-64.
9. Ishizawa T, Fukushima N, Shibahara J, et al. Real-time identification of liver cancers by using indocyanine green fluorescence imaging. *Cancer* 2009; 115:2491-504.
10. Gutowski M, Carcenac M, Pourquier D, et al. Intraoperative immunophotodetection for radical resection of cancers: evaluation in an experimental model. *Clin Cancer Res* 2001; 7:1142-8.
11. De Grand AM, Frangioni JV. An operational near-infrared fluorescence imaging system prototype for large animal surgery. *Technol Cancer Res Treat* 2003; 2:553-62.
12. Kitai T, Inomoto T, Miwa M, Shikayama T. Fluorescence navigation with indocyanine green for detecting sentinel lymph nodes in breast cancer. *Breast Cancer* 2005; 12:211-5.
13. Ke S, Wen X, Gurfinkel M, et al. Near-infrared optical imaging of epidermal growth factor receptor in breast cancer xenografts. *Cancer Res* 2003; 63:7870-5.
14. Kirsch DG, Dinulescu DM, Miller JB, et al. A spatially and temporally restricted mouse model of soft tissue sarcoma. *Nat Med* 2007; 13:992-7.
15. Troyan SL, Kianzad V, Gibbs-Strauss SL, et al. The FLARE intraoperative near-infrared fluorescence imaging system: a first-in-human clinical trial in breast cancer sentinel lymph node mapping. *Ann Surg Oncol* 2009; 16:2943-52.
16. Murawa D, Hirche C, Dresel S, et al. Sentinel lymph node biopsy in breast cancer guided by indocyanine green fluorescence. *Br J Surg* 2009; 96:1289-94.
17. Noura S, Ohue M, Seki Y, et al. Feasibility of a lateral region sentinel node biopsy of lower rectal cancer guided by indocyanine green using a near-infrared camera system. *Ann Surg Oncol* 2010; 17:144-51.
18. Soltesz EG, Kim S, Kim SW, et al. Sentinel lymph node mapping of the gastrointestinal tract by using invisible light. *Ann Surg Oncol* 2006; 13:386-96.
19. Tanaka E, Choi HS, Fujii H, et al. Image-guided oncologic surgery using invisible light: completed pre-clinical development for sentinel lymph node mapping. *Ann Surg Oncol* 2006; 13:1671-81.
20. Matsui A, Lee BT, Winer JH, et al. Image-guided perforator flap design using invisible near-infrared light and validation with x-ray angiography. *Ann Plast Surg* 2009; 63:327-30.
21. Weissleder R, Tung CH, Mahmood U, Bogdanov A, Jr. In vivo imaging of tumors with protease-activated near-infrared fluorescent probes. *Nat Biotechnol* 1999; 17:375-8.
22. Marquet RL, Westbroek DL, Jeekel J. Interferon treatment of a transplantable rat colon adenocarcinoma: importance of tumor site. *Int J Cancer* 1984; 33:689-92.
23. van Dierendonck JH, Keijzer R, Cornelisse CJ, et al. Surgically induced cytokinetic responses in experimental rat mammary tumor models. *Cancer* 1991; 68:759-67.
24. Wijsman JH, Cornelisse CJ, Keijzer R, et al. A prolactin-dependent, metastasising rat mammary carcinoma as a model for endocrine-related tumour dormancy. *Br J Cancer* 1991; 64:463-8.
25. Lopes Cardozo AM, Gupta A, Koppe MJ, et al. Metastatic pattern of CC531 colon carcinoma cells in the abdominal cavity: an experimental model of peritoneal carcinomatosis in rats. *Eur J Surg Oncol* 2001; 27:359-63.
26. Rasband WS. ImageJ, U. S. National Institutes of Health, Bethesda, Maryland, USA, <http://rsb.info.nih.gov/ij/>. 2009.

27. Keppler D, Walter R, Perez C, et al. Increased expression of mature cathepsin B in aging rat liver. *Cell Tissue Res* 2000; 302:181-8.
28. Todorov V, Muller M, Kurtz A. Differential regulation of cathepsin B and prorenin gene expression in renal juxtaglomerular cells. *Kidney Blood Press Res* 2001; 24:75-8.
29. Mohamed MM, Sloane BF. Cysteine cathepsins: multifunctional enzymes in cancer. *Nat Rev Cancer* 2006; 6:764-75.
30. Harbeck N, Alt U, Berger U, et al. Prognostic impact of proteolytic factors (urokinase-type plasminogen activator, plasminogen activator inhibitor 1, and cathepsins B, D, and L) in primary breast cancer reflects effects of adjuvant systemic therapy. *Clin Cancer Res* 2001; 7:2757-64.
31. Parker BS, Ciocca DR, Bidwell BN, et al. Primary tumour expression of the cysteine cathepsin inhibitor Stefin A inhibits distant metastasis in breast cancer. *J Pathol* 2008; 214:337-46.
32. Kuester D, Lippert H, Roessner A, et al. The cathepsin family and their role in colorectal cancer. *Pathol Res Pract* 2008; 204:491-500.
33. Rosenfeld A, Kak A. *Digital picture processing*. 2nd edn. New York: Academic Press; 1982.
34. Kumar AT, Raymond SB, Bacskai BJ, et al. Comparison of frequency-domain and time-domain fluorescence lifetime tomography. *Opt Lett* 2008; 33:470-2.
35. Gioux S, Mazhar A, Cuccia DJ, et al. Three-dimensional surface profile intensity correction for spatially modulated imaging. *J Biomed Opt* 2009; 14:034045.